Conformational preferences of the flexible galactofuranose sugar in gas-phase

Oznur Yeni, Abdul-Rahman Allouche, Laurent Legentil, Vincent Ferrières, Isabelle Compagnon

Conformational preferences of the flexible galactofuranose sugar in gas-phase

Oznur Yeni,[a] Abdul-Rahman Allouche, [a] Laurent Legentil, [b] Vincent Ferrières [b] and Isabelle Compagnon *[a]

In contrast with the predominant pyranose form of galactose, galactofuranose is known to be highly flexible. Such flexibility poses a remarkable challenge in terms of structural studies, thus hindering the in depth understanding of the structure/function relationship in this rare sugar. A thorough computational study based on molecular dynamics and density functional theory supported by vibrational spectroscopy in the gas phase was carried out to provide a better understanding of the instrinsic conformational preferences of galactofuranose. Based on energetic and spectroscopic criteria, we report a substantially reduced conformational landscape: methyl α-D-galactofuranose adopts $E_2/{}_1E$ conformations and methyl β-D-galactofuranose adopts ${}_1T_2/{}_1E$ conformations.

Introduction

Galactose is a widely spread hexose in nature and may be present in both pyranose (6-membered ring) and furanose form (5-membered ring). Mammals can only biosynthesize galactose units in the pyranose configuration, whereas the furanose form is found in fewer organisms such as bacteria, parasites, fungi, plants and lichens.[1–3] This minute structural variation at the atomic scale has two major implications in biology: on one hand the energetic cost for the biosynthesis of a five-membered ring hexose is higher; on the other hand it offers more conformational freedom than its six-membered ring counterpart.[4,5] This leads to many biological questions: why do these species prefer to biosynthesize the galactofuranose form at a higher cost? How does the flexibility affect the physical and chemical properties of galactofuranose-containing polysaccharides? Does it enable unique biological functions?

In this context, a better understanding of the structural properties of furanosides is essential in order to gain a deeper understanding of its biological impact. This endeavour requires paramount, interdisciplinary efforts to combine challenging chemical synthesis of well-defined furanose-containing standards;[3,6–9] extensive and accurate potential energy surface exploration; spectroscopic techniques offering structural resolution at the atomic scale; and finally high level quantum chemistry methods with sufficient precision to match spectroscopic data. Ten years ago, Lowary reviewed such approaches, going back as far as the 60's in the case of the most studied hexofuranose: fructose.[10] In the case of galactofuranose, he reported that the ring can adopt several conformations separated by low energy barriers due to the high ring strain and the large number of rotamers differing by OH orientation. In contrast, pyranose rings generally adopt the ubiquitous, low energy ${}^4C_1$ chair conformation, which is stabilized by a fully coordinated hydrogen bonds network. The challenge of the furanose ring conformation was highlighted in a reference study where a conformational analysis on individual anomers of methyl D-galactofuranoside carried out in solution using NMR spectroscopy, densityfunctional theory (DFT) and proton–proton coupling constant analysis with PSEUROT[11] indicated a ${}_2E$ envelope conformation for methyl a-D-galactofuranoside (αGalfOMe), but could not provide conclusive results regarding methyl β-D-galactofuranoside (βGalfOMe). Gerbst et al. reported alternative conformations of galactofuranoside derivatives using different DFT functionals and MP2 approaches.[12]

Gas phase spectroscopy in combination with quantum calculations constitutes an alternative approach, where the absence of environment conveniently allows examining the intrinsic conformational properties driven by intramolecular H-bonds networks; or even to investigate the influence of micro-environment (one solvent molecule, a charge…). A number of authors have reported gas-phase spectroscopy of sugars using various spectroscopic schemes, such as infrared (IR) and microwave (MW) in neutral jets. For example, MW was used to investigate the bare molecules fructose[13] and α-D-galactopyranose.[14] Galactopyranose derivatives were also analysed in different micro-environment such as complexed to a peptide sensor (a- and β-methyl D-galactopyranoside)[15] or micro-solvated (phenyl β-D-galactopyranoside).[16] These approaches offer the possibility to derive very accurate conformations with the support of high-level theoretical calculations.

Others have coupled gas phase infrared spectroscopy with mass spectrometry (MS) for the study of ionic species: IRMPD spectroscopy (InfraRed Multiple Photon Dissociation),[17] IR spectroscopy in helium droplet[18] and IR messenger-tagging spectroscopy,[19] as recently reviewed in.[20] In addition to providing experimental data to derive conformations, spectroscopy coupled to mass spectrometry has the advantage to extend the analytical capabilities of MS by offering distinctive signatures of sugar isomers.

However, much less conformational studies of furanoses have been reported, including ribose, deoxyribose and Galf-NAc.[21–23] Recently, we have published two experimental IRMPD studies on galactose (methyl α-D-galactofuranoside, methyl β-Dgalactofuranoside and their pyranose counterparts methyl α-D-galactopyranoside and methyl β-D-galactopyranoside) and on galactose-containing disaccharides (β-D-galactofuranose(1-x)Mannose, x = 2, 3, 4 or 6 and their counterpart β-D-galactopyranose (1-x)Mannose).[24,25] Due to the absence of acidic or basic group, such sugars could not be detected in the protonated or deprotonated states. Therefore, they were complexed with NH_4^+ or Li^+. We reported that galactofuranoses and galactopyranoses feature distinctive IRMPD spectra, regardless of the charge carriers. This is very intriguing because we do not usually expect to observe resolved spectroscopic features for flexible molecules using IRMPD.[26] The case of NH_4^+ complexes was particularly interesting because the galactofuranoses and galactopyranosesmonosaccharides spectra were highly contrasted in the 3 mm spectral range (range of the OH stretching vibration), that is dominated by a single and intense band for α- and β-galactofuranose O-methylated, whereas their galactopyranosidic counterparts feature a well identifiable doublet of bands in the same area.

Remarkably, this spectroscopic diagnostic of the ring size of galactose was also observed in galactose-containing disaccharides, suggesting that the conformational preferences of the monosaccharide translate to larger molecules. The ambition of this work is to use high-level quantum chemistry to interpret these analytical findings and to provide better insight in the conformational preference of the galactofuranose ion in the gas-phase. To that end, we present the first conformational analysis of galactofuranose supported by gas phase IR spectroscopy. We report that both E_2 and ^2E are energetically favourable in the case of the a-anomer, and can be discriminated based on a spectroscopic criterion, showing an intrinsic preference for the E_2 conformation. In the case of the β-anomer, our data suggest a marked preference for conformers centered around the closely related ^1E envelope and $^1T_2$ twist conformations. We expect that these results provide valuable structural data for the future development of in silico models of furanosylcontaining polysaccharides, and more generally a pertinent approach for the structural analysis of highly flexible or disordered molecules.

Materials and methods

Methyl α-D-galactopyranoside (αGalpOMe) and methyl β-Dgalactopyranoside (βGalpOMe) were purchased from Carbosynth. Methyl α-D-galactofuranoside (αGalfOMe) and methyl β-D-galactofuranoside (βGalfOMe) were synthetized by the method detailed in.[24] Their structures are represented in Scheme 1. The four monosaccharides were ionized in an electrospray ion source (ESI†) with a NH_4^+ adduct, and their IRMPD signatures were previously recorded.[24]

Molecular dynamics (MD) was used to explore the potential energy surface of each ion with the PM7 potential in OpenMopac.[27] For each starting structure, a trajectory of 10 ps at 1000 K was ran and generated 20 000 individual geometries. A virtual trapping potential was added to PM7 to ensure that the weakly bonded NH_4^+ adduct freely explores all possible complexation sites of the sugar but won't evaporate during the run. This custom modification was previously described in ref. 28. Note on the chosen representations: the conformations of six-membered rings are generally represented using the Cremer–Pople (C–P) parameters j and y.[29,30] For five-membered rings however, several representations have been proposed. Altona–Sundaralingam, which exploits the two coordinates pseudorotation phase P and pseudorotation

amplitude j_m;[31] and Cremer–Pople which uses cartesian coordinates are often – but not exclusively – used.[30] In the following discussion, we used C–P for six-membered rings and A–S for five-membered rings.

The MD trajectories are shown in Fig. 1 (in grey). To assess the quality of the exploration of the potential energy surface (PES), we verify that the trajectory occupies all regions of the map. Here the five-membered ring PES is satisfactorily explored including the puckering of the ring; the rotation of the OH groups, and the location of the charge.

Two stages of DFT calculations were then used to refine the structure and energy. A first optimization of the MD geometries was first carried out using B3LYP/6-31G method,[32–34] yielding new starting structures for a second stage of DFT calculations at the CAM-B3LYP/6-311++G(2df,2pd) level.[35] The simulation of the harmonic vibrational frequencies was carried out at the same level. An empirical scaling factor of 0.947 was used to account for anharmonic effects and for comparison with the gas phase IR spectra. At each stage of the analysis, identical structures (based on geometry and energy criteria) are deleted before seeding the next level of calculations. The results are analysed with Gabedit.[36]

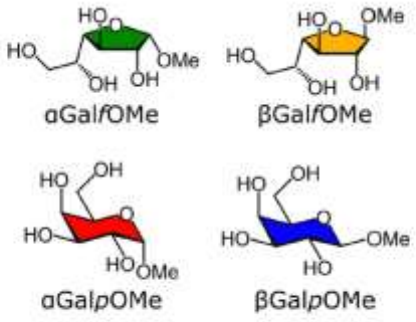

Scheme 1 Structures of methyl α-D-galactofuranoside (αGal*f*OMe), methyl β-D-galactofuranoside (βGal*f*OMe), methyl α-D-galactopyranoside (αGal*p*OMe) and methyl β-D-galactopyranoside (βGal*p*OMe)

Results

Conformational exploration

20 000 conformations were generated by MD for each of the four models. Their coordinates are reported in Fig. 1 (grey dots) using Altona–Sundaralingam parameters for 5-membered rings (P is represented by the angular coordinate and j_m by the axial coordinate) or Cremer–Pople for 6-membered rings (j is represented by X-axis and y by Y-axis). The thread of individual structures can naturally be interpreted as the trajectory followed by the ion during the MD simulation. As seen in the Altona–Sundaralingam wheels, the furanose structures cover the entirety of the surface, which validates that the conformational space was meticulously explored. Note that the wheels only represent the puckering angles, thus the conformation of the ring, and do not account for the other important parameters of the exploration, i.e. the OH rotamers and the localization of the NH_4^+ adduct. This point was validated by visual inspection and a random selection of conformations exhibiting different NH_4^+ positions and rotations of the OH groups are shown in Fig. S1 (ESI†) for illustration. Note that at the MD stage, the energies are not considered. Two stages of DFT calculations were then used to optimize the structures and calculate their energy. During DFT optimization, entire subset of crude MD structures may converge towards a unique stable conformation, resulting in a fewer number of structures. In particular, stable furanose rings tend to concentrate in the outer area of the wheel (high j_m values) and stable pyranose rings tend to concentrate around y = 01, 901 and 1801. The coordinates of the different structures after CAM-B3LYP optimization are reported in Fig. 1 in green for αGalfOMe, orange for βGalfOMe, red for αGalpOMe and blue for βGalpOMe (the intermediate B3LYP distribution is not shown for clarity). For αGalfOMe, a good distribution of the pseudorotational phase P can be noticed, except the unpopulated section from 225 to 2551. This region corresponds to conformations with 4C above the ring formed by O1–C1–C2–C3 (0 ^4T_O, 0 ^4E and only 2 $^4T_3$ are present among 250 most stable conformations). The position of

OMe on anomer β disfavors other configurations: 296 more stable structures with CAMB3LYP calculations do not include configuration with C1 below the ring plane ($_0T_1$ or E_1). The main reason is the difficulty to have O1Me involved in a hydrogen bond with an equatorial orientation. Thus, the disfavored conformations differ according to the anomericity. For both pyranoses, the optimization by CAM-B3LYP leads to conformations with y close to 01, 901 or 1801, which corresponds to the $^4C_1$, the range of B and S forms, and $^1C_4$ forms, respectively.

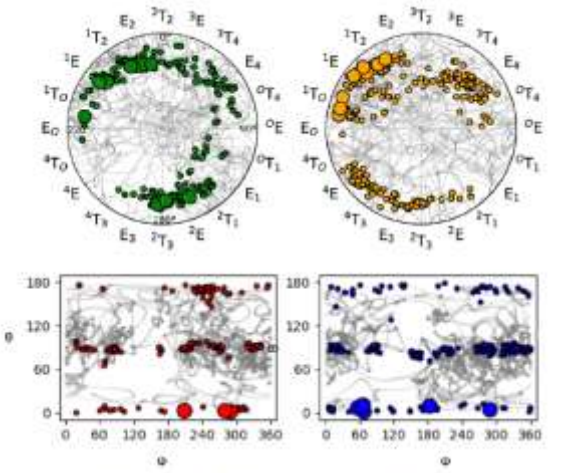

Fig. 1 Coordinates of each conformer obtained during the MD trajectory for αGalfOMe (upper left wheel), βGalfOMe (upper right wheel), αGalpOMe (bottom left map) and βGalpOMe (bottom right map) represented in grey. Coordinates of each conformer after CAMB3LYP optimization (αGalfOMe: 250 conformations represented in green, βGalfOMe: 296 conformations in orange, αGalpOMe: 212 conformations in red and βGalpOMe: 231 conformations in blue). The larger dots represent the subset of conformations under the energy cut-off (αGalfOMe: 12 conformations, βGalfOMe: 13 conformations, αGalpOMe: 3 conformations and βGalpOMe: 3 conformations). Their relative energies are reported in Fig. 2.

Energetic criterion

The energy of each conformer was calculated at the CAMB3LYP/6-311++G(2df,2pd) level of theory. A selection of low energy structure is made for each of the four models using an energy cut-off of 8.3 kJ mol_1, which corresponds to a thermal energy of ca. 1000 K. The relative energies of these low-lying structures are represented in Fig. 2, using the minimum minimorum, i.e. the lowest αGalpOMe conformer, as a reference. Only 3 conformations for αGalpOMe and 3 for βGalpOMe were found in the 8.3 kJ mol_1 energy window. Unsurprisingly, all methyl pyranoside conformers adopted a $^4C_1$ chair conformation. In contrast, many different furanose conformers exist under 8.3 kJ mol_1: 12 for αGalfOMe and 13 for βGalfOMe. These stable structures are highlighted on Fig. 1 with larger dots. For αGalfOMe, they are located in northwest and south regions of the wheel whereas only northwest is populated in the case of βGalfOMe.

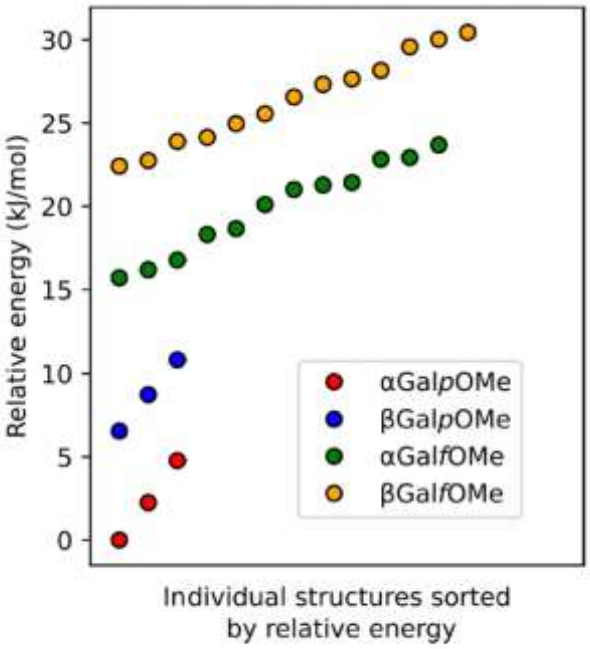

Fig. 2 Relative CAMB3LYP energy of lowest energy structures for αGal-*p*OMe (red), βGal*p*OMe (blue), αGal*f*OMe (green) and βGal*f*OMe (yellow) corresponding to the large dots in Fig. 1.

Galactopyranoside conformational preferences

The lowest energy structures of aGalpOMe and bGalpOMe are shown in Fig. 3 and are compared with the experimental IRMPD spectra. They both adopt a $^4C_1$ chair conformation. The position of NH_4^+ is the same for both structures: it intercalates between O3H and O4H. The NH_4^+ adduct thus participates in a fully coordinated hydrogen network OH6–HO4–HNH–O3H–O2H (–O1Me for anomer a). This is in agreement with previously published hexopyranose/cationic adduct complexes.[28] The calculated IR spectra of these two structures are in excellent agreement with the experimental spectra, with the exception of the modes that are involved in strong H-bond, which are generally discarded in the analysis (here the O4H mode). The rest of the vibrations are interpreted as follows: both structures share a common CH range between 2800 and 3000 cm_{-1} that account for the broad experimental feature in this region. H-bonded NH modes around 2730 and 3020 cm_{-1} accounts for the absorption background lying under the CH region. Two other NH modes at 3390 and 3400 cm_{-1} match with the two experimental features. Calculated OH modes present also similitudes for both anomers: the free O6H frequency is calculated at 3650 cm_{-1}; O4H is strongly H bonded to O6H and is redshifted (3250 cm_{-1}, not observable experimentally); and O3H weakly bonded to O2H is calculated at 3560 cm_{-1} for αGalpOMe and 3590 cm_{-1} for βGalpOMe, which shows a good agreement with the feature at 3580 cm_{-1} present in both experimental spectra. The major difference between the two simulated spectra consists in O2H frequency.

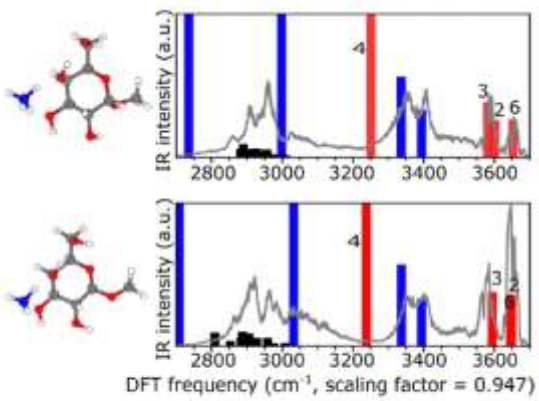

Fig. 3 Structure of the most stable conformations of αGalpOMe (top) or βGalpOMe (down) and their vibrational modes of OH (red), NH (blue) and CH (black). The labels indicate the ring OH position. The experimental spectra are shown in grey.

For αGalpOMe, its frequency is calculated at 3600 cm_{-1} and for βGalpOMe it appears at 3650 cm_{-1}. This can be explained by the position of O1Me. For α-anomer, O2H and O1Me are on the same plan, below the plane of the ring, allowing a hydrogen bond. In contrast, O1Me is above the ring, which does not permit the hydrogen bonding O2H—OMe for the β-anomer. This is confirmed experimentally by the relative intensity of the two OH bands: the experimental feature at 3600 cm_{-1} is higher for αGalpOMe (corresponding to both O2H and O3H frequencies) whereas the feature at 3650 cm_{-1} is higher for βGalpOMe (O2H and O6H frequencies). The excellent match between simulated and experimental spectra validates that αGalpOMe and βGalpOMe adopt a $^4C_1$ conformation with the NH_4^+ adduct localized between O3H and O4H and are stabilized by a fully coordinated hydrogen-bond network in our experimental conditions, that is at room temperature and in absence of solvent. Other low energy structures featuring a different position of the NH_4^+ or other rotamers of the $^4C_1$ might be present in minor amount and could explain the weak absorption around 3500 cm_{-1} (See Fig. S2 and S3 in ESI†). While these results are not surprising, they validate the relevance of the approach, which can further be used to elucidate the conformational preference of the more challenging galactofuranosides.

Galactofuranoside conformational preferences

Many conformers are found within 8.3 kJ mol_{-1} and the energy gap between them are very low. Their structures and calculated frequencies are shown in Fig. S4 (ESI†) for αGalfOMe and Fig. S5 (ESI†) for βGalfOMe. They adopt various ring conformations: 5 for the a-anomer (namely E_2, E_O, $_2T_3$, $_1E$ and $_2E$) and 3 for the β-anomer (namely $_1T_2$, $_1T_O$ and $_1E$). Each family feature different rotamers (variations of the dihedral angles of the OH groups) and their IR calculated spectra are very similar. One rotamer of each category is represented in Fig. 4 for αGalfOMe and Fig. 5 for βGalfOMe.

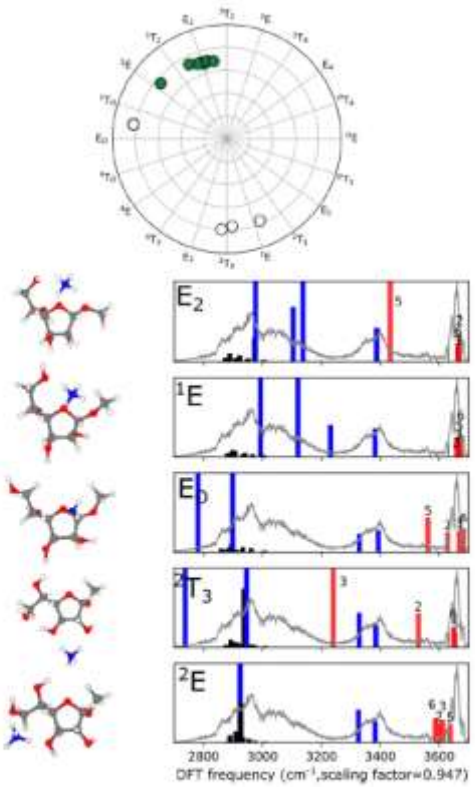

Fig. 4 Upper wheel: coordinates of the most stable structures (under 8.3 kJ mol^{-1}) on a phase/amplitude conformational wheel for αGalfOMe. Lower panels: structures of the most stable conformations and their vibrational modes of OH (red), NH (blue) and CH (black) compared to the experimental spectrum (grey). The labels indicate the ring OH position. One typical structure for each ring conformation is represented (see ESI† for other rotamers). Structures eliminated by comparison of calculated/experimental spectra were whited out on the wheel.

αGalfOMe. E_2 conformers are characterized by a strong H-bond O5H–O2, resulting in a redshift of the O5H calculated frequency (between 3400 and 3430 cm_{-1}). One NH band appears at 3390 cm_{-1}. A single conformer with lower energy adopts $_1E$ geometry type where all OH groups are free, resulting in high calculated frequencies around 3670 cm_{-1}. As for E_2 conformers, one NH stretching mode is calculated at 3390 cm_{-1}. E_O conformers are characterized by O5H oriented and bonded to O6, which leads to a redshift of O5H around 3550 cm_{-1}. Some conformers adopt southern geometry types. $_2T_3$ geometry type is stabilized by a NH_4^+ located between O2H and O3H. This results in a strong bond O3H–O5H for one part and O2H–O1 for the other part. For $_2E$ conformation, NH_4^+ is located between O3H and O5H. All OH groups are weakly bonded, which results in a redshift of their frequencies around 3600 cm_{-1}. The experimental spectrum agrees well with some Northern conformers: the experimental band observed at 3650 cm_{-1} matches with free OH of E_2 and $_1E$ conformers. It is expected that highly bonded modes have a low intensity and may not be experimentally observed, such as O5H mode of E_2 conformer calculated around 3410 cm_{-1}. On the contrary, free or low bonded modes are experimentally observed. Thus, E_O and southern conformations $_2T_3$ and $_2E$ can be excluded because there are no experimental features between 3530 and 3600 cm_{-1}.

βGalfOMe. In contrast, the lowest energy structures of βGalfOMe only adopt Northwest conformations: only $_1T_2$, $_1E$ and $_1T_O$ conformers were found (Fig. 5). $_1T_2$ conformers are characterized by a strong OH5–O2H hydrogen bond behind the ring plane and a weak OH3–O1Me in front of the ring plane. NH_4^+ position affects the H-bonds of some conformers. Two conformers adopt $_1E$ conformation, they form a OH3–OMe bond such for $_1T_2$ conformers and differ by the absence of H-bond beside the ring (O5H is free). The difference between

these two conformers is O6H rotation. For $_1T_O$ conformers, O5H is oriented towards O6 allowing a H-bond between these two groups. Thus, O5H frequency is redshifted around 3530–3560 cm$_{-1}$. By comparing with the experimental spectrum, we can conclude that $_1T_2$ and $_1E$ conformers calculated spectra match perfectly: the intense band at 3650 cm$_{-1}$ corresponds to free OH groups; calculated O3H frequencies may explain the weak band at 3600 cm$_{-1}$ and the two NH bands at 3350 and 3400 cm$_{-1}$ match with the calculated NH modes. By opposition, $_1T_O$ conformers can be ruled out because of the absence of experimental band at 3550 cm$_{-1}$.

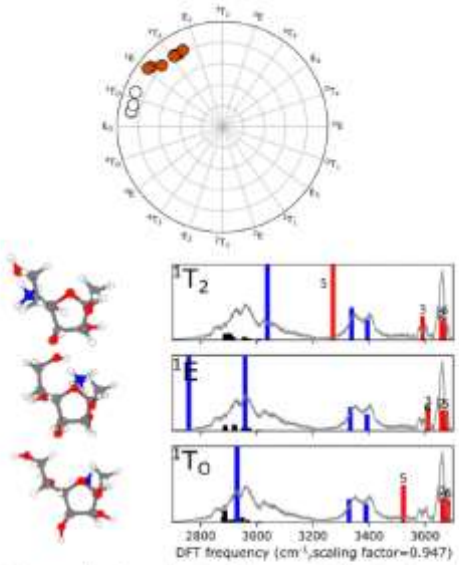

Fig. 5 Upper wheel: coordinates of the most stable structures (under 8.3 kJ mol^{-1}) on a phase/amplitude conformational wheel for βGalfOMe. Down: structures of the most stable conformations and their vibrational modes of OH (red), NH (blue) and CH (black) compared to the experimental spectrum (grey). The labels indicate the ring OH position. One typical structure for each ring conformation is represented (see ESI† for other rotamers). Structures eliminated by comparison of calculated/experimental spectra were discoloured on the wheel.

Discussion

We ran conformational surface exploration and simulated IR spectra of the well-established $_4C_1$ galactopyranose ring as a reference to validate the precision of our simulation pipeline against gas phase spectroscopy data. This approach was then deployed to elucidate the intrinsic conformational preferences of galactofuranosides in the same conditions. We verified that the ring-size and anomericity affect the molecule stability. There is a difference of 15 kJ mol$_{-1}$ between pyranoses and furanoses at the DFT CAM-B3LYP level of theory. This finding is in accordance with the state-of-the-art knowledge about furanoses, known to be thermodynamically less stable than pyranoses. We also report the difference of internal energies according to the anomericity: α anomers are more stable for both ring size (difference of 5 kJ mol$_{-1}$). The energetics suggests that αGalfOMe is present in the Northwest (E_2, E_O and $_1E$) and South ($_2T_3$ and $_2E$) regions of the Altona–Sundaralingam wheel, which is consistent with the $_2E$ conformation observed by NMR.[11] Surprisingly, βGalfOMe which could not be conclusively captured in NMR studies seems to occupy a more restricted conformational space with only Northwest conformations ($_1T_2$, $_1T_O$ and $_1E$).

Flexible molecules pose a particular challenge to theoreticians and spectroscopists altogether because when several conformations coexist or interconvert, one expects a critical broadening of the spectroscopic features, thus a loss of diagnostic information. This is particularly true in the case of solution phase spectroscopy because the solvent tends to disrupt the stabilizing intermolecular H-bond network and to facilitate interconversion. As a matter of fact, the H-bond network was not taken into account in the interpretation of the NMR data in previous galactofuranosides studies. An advantage of the gas phase spectroscopy is to unravel the intrinsic conformational preferences of molecules in absence of environment,

and the fine tuning of their properties in the presence of micro-environment (a charged amino group in,[23] a NH_4^+ adduct in the present study). We have reported surprisingly well resolved gas phase IR spectra, which revealed an important diagnostic: furanosides display one intense OH feature at 3650 cm^{-1} whereas their pyranosides counterparts also show a second intense OH feature at 3600 cm^{-1}. These experimental features allow further discrimination of the energetically favourable conformation.

Using this additional criterion, we could rule out the $^1T_0$ conformation of βGalfOMe, whose populated space in our room temperature condition come down to the two closely related $^1T_2$ and ^1E forms. In the case of αGalfOMe, a quite surprising effect is reported: both Northwest and South populations are energetically populated, but the spectroscopic criterion indicates that only the Northwest area is actually populated, in particular the E_2 and ^1E forms, in striking contrast with the South (^2E) form observed in solution. In this study, we show that in the gas phase both galactopyranose anomers are involved in a hydrogen network, resulting in two experimental OH bands: one corresponding to free OH and the other one, redshifted, to weakly bonded OH groups. The relative intensity of these two bands is linked to the anomericity: α-anomer has a ratio intensity of bonded OH/free OH band more important than βGalfOMe due to the O2H–OMe bond which exists only for α-anomer. Less hydrogen bonds occur in furanose structures, resulting in an intense OH band corresponding to free OH. A second weak OH band at 3600 cm^{-1} can be observed only for β-anomer because, as for pyranoses, the anomericity affects hydrogen bonds. Indeed, only β form displays the hydrogen bond O3H–OMe, resulting in a redshift of O3H mode around 3600 cm^{-1}.

While it is common sense that the micro-environment has a critical influence on the conformational behaviour of flexible molecule, it remains extremely challenging to develop adequate experimental and theoretical tools to rationalise the role of intrinsic and external factors. The case of furanosides is particularly daunting because any variation of the environment critically affects the conformation of the ring: Cocinero **et al.** have reported $^3T_2$ conformation for methyl β-D-ribofuranoside[21] whereas the methyl 2-deoxyribofuranoses in gas phase adopts $^2T_1$ conformation (α-anomer) or $^4E/E_2/^1T_2$ conformations (β-anomer).[22] Gerbst **et al.** reported structures ranging from E_0/E_2 to $E_3/^4E$ for lactic acid- and propyl-galactofuranosides in solution;[12] Lowary **et al.** highlighted the elusive character of βGalfOMe whereas the same conditions yielded conclusive ^2E data for αGalfOMe.[11] Strikingly, the later essentially adopts E_2 conformations in the gas phase, in contrast to the Southwest gas phase conformations previously reported for the N-acetylated galactofuranosides.

In this context, gas phase spectroscopy in the 3 mm spectral range is a tool of choice because it covers the OH vibrational modes, whose exact frequency is extremely responsive to the presence and strength of intramolecular as well as intermolecular (here the NH_4^+ adduct) H-bonds. Hence it offers a highly specific probe of the intrinsic conformational preference of a molecule and is at the same time suitable to probe microenvironment effects.

Our results demonstrate that a very restricted group of furanose conformers are experimentally present. When several conformations coexist or interconvert, one expects a critical broadening of the spectroscopic features, thus a loss of information in an analytical prospective. But surprisingly highly resolved spectra were obtained. These experimental features justified a gas-phase spectroscopic approach: the combination of energetic and spectroscopic arguments allows unravelling the intrinsic conformational preferences and rationalizing this direct diagnostic of the ring size. The fact that both anomers of galactofuranoside adopt Northwest geometries in the gas phase ($E_2/^1E$ for anomer α and $^1T_2/^1E$ for anomer β), while previous studies reported South conformations, reinforces the chemical intuition concerning the subtle balance of intramolecular and intermolecular forces at play in highly flexible molecules. In contrast, pyranosides generally adopt chair conformations regardless of the environment. For example, MW study on the neutral α-galactopyranose in gas-phase had shown 4 conformers with $^4C_1$ in gas-phase,[14] our analysis also reported $^4C_1$ conformation for the complexe with NH_4^+. It is acknowledged that the environment can induce conformational changes,[37] especially for five-membered ring which are highly dependent on the environment

because of the charge flux induced by the solvent.[38] On the other hand, gas phase studies shed light on the intramolecular effects and our spectroscopic approach in the mid-IR range specifically enables the description of the intramolecular H-bond network: in particular, the exact frequency of the OH stretching vibration can reveal the involvement of each individual hydroxyl group of the molecule in a H-bond.
We report that both galactopyranosidic anomers accommodate a dense H-bond network, resulting in two experimental OH features: one corresponding to free OHs at 3650 cm_{-1} and a strong one at 3600 cm_{-1} corresponding to H-bonded OH groups. The relative intensity of these two bands reveals the anomericity: the α-anomer has a higher intensity ratio of H-bonded OH/free OH than βGalfOMe because the O2H–OMe H-bond can only be formed in the α-anomer. In contrast, the formation of stabilizing H-bonds is not favoured by the five-membered ring, which results in the intense free OH feature observed experimentally at 3650 cm_{-1}. In the case of βGalfOMe, a unique H-bond can be formed across the ring between O3H and O1, resulting in the weak experimental feature observed at 3600 cm_{-1}.

Conclusions

In this study, we addressed the conformational preferences of methyl α-D-galactofuranoside, methyl β-D-galactofuranoside,methyl α-D-galactopyranoside and methyl β-D-galactopyranoside, as ammonium adduct, in the gas phase, using a combination of IR spectroscopy in the highly diagnostic OH vibration range, extensive molecular dynamics and quantum chemistry simulations at the DFT CAM-B3LYP/6-311++G(2df,2pd) level of theory. This approach is validated by verifying that it yields the expected $^4C_1$ conformation stabilized by a full coordination of hydroxyl groups in the case of the pyranose forms. The same computational study has been carried out on galactofuranose and has shed new light on its conformational preferences: it adopts very restricted range of energetically close conformations in the Northwest region, specifically E_2 and $_1E$ formethyl α-D-galactofuranoside and $_1T_2$ to $_1E$ for methyl β-D-galactofuranoside. To the best of our knowledge, this is the first conclusive report of the previously elusive conformation of the β–anomer of galactofuranoside. At the DFT CAM-B3LYP/6-311++G(2df,2pd) level of theory, it was possible to describe the intramolecular H-bond network (or its absence), which adds an original angle to the state of the art. In addition, we proposed a rationalization of the IR diagnostic of the ring size, which was previously reported in monosaccharides and disaccharides standards in an analytical context.[24,25] The combination of gas phase IR spectroscopy with high level quantum chemistry offered an unprecedented level of description of the conformation of galactofuranoses. However, the performance of such approach is not readily applicable to large size system. Yet, one can ambition to use these structural data to derive high quality parameters an develop accurate force fields dedicated to furanosyl-containing polysaccharides.[39] Such developments would certainly bring new insights in the structure–function relationship and the biological function of these rare sugars. More generally, we expect that this work opens exciting prospective concerning the structural properties of highly flexible molecules.

Author contributions

O. Y.: investigation, visualization, writing – original draft, writing – review & editing. A-R. A., L. L.: resources. V. F.: resources, funding acquisition, supervision. I. C.: conceptualization, funding acquisition, supervision, writing – original draft, writing – review & editing.

Conflicts of interest

There are no conflicts to declare.

Acknowledgements

The authors thank Laura L. Kiessling for stimulating discussions, the Agence Nationale de la Recherche (ANR) for financially supporting the ALGAIM-MS project (ANR-18-CE29-0006-02, https://algaims-35.webself.net/accueil). This work was granted access to the HPC resources of the ‘‘Centre de calcul CC-IN2P3’’ at Villeurbanne, France.

Notes and references

1 L. L. Pedersen and S. J. Turco, Cell. Mol. Life Sci., 2003, 60, 259–266.
2 B. Tefsen, A. F. Ram, I. van Die and F. H. Routier, Glycobiology, 2012, 22, 456–469.
3 P. Peltier, R. Euzen, R. Daniellou, C. Nugier-Chauvin and V. Ferrieres, Carbohydr. Res., 2008, 27.
4 M. Levitt and A. Warshel, J. Am. Chem. Soc., 1978, 100, 2607–2613.
5 W. K. Olson and J. L. Sussman, J. Am. Chem. Soc., 1982, 104, 270–278.
6 T. Lowary, Curr. Opin. Chem. Biol., 2003, 7, 749–756.
7 M. R. Richards and T. L. Lowary, ChemBioChem, 2009, 10, 1920–1938.
8 T. L. Lowary, Acc. Chem. Res., 2016, 49, 1379–1388.
9 A. L. Marlow and L. L. Kiessling, Org. Lett., 2001, 3, 2517–2519.
10 H. A. Taha, M. R. Richards and T. L. Lowary, Chem. Rev., 2013, 113, 1851–1876.
11 M. R. Richards, Y. Bai and T. L. Lowary, Carbohydr. Res., 2013, 374, 103–114.
12 A. G. Gerbst, V. B. Krylov and N. E. Nifantiev, Front. Mol. Biosci., 2021, 8, 719396.
13 E. J. Cocinero, A. Lesarri, P. E´ cija, A´. Cimas, B. G. Davis, F. J. Basterretxea, J. A. Ferna´ndez and F. Castan˜o, J. Am. Chem. Soc., 2013, 135, 2845–2852.
14 I. Pen˜a, C. Cabezas and J. L. Alonso, Chem. Commun., 2015, 51, 10115–10118.
15 E. J. Cocinero, P. Carcabal, T. D. Vaden, J. P. Simons and B. G. Davis, Nature, 2011, 469, 76–79.
16 J. P. Simons, R. A. Jockusch, P. CarCabal, I. Hu¨nig, R. T. Kroemer, N. A. Macleod and L. C. Snoek, Int. Rev. Phys. Chem., 2005, 24, 489–531.
17 B. Schindler, L. Barnes, G. Renois, C. Gray, S. Chambert, S. Fort, S. Flitsch, C. Loison, A.-R. Allouche and I. Compagnon, Nat. Commun., 2017, 8, 1–7.
18 E. Mucha, A. Stuckmann, M. Marianski, W. B. Struwe,

G. Meijer and K. Pagel, Chem. Sci., 2019, 10, 1272–1284.
19 C. Masellis, N. Khanal, M. Z. Kamrath, D. E. Clemmer and T. R. Rizzo, J. Am. Soc. Mass Spectrom., 2017, 28, 2217–2222.
20 M. Grabarics, M. Lettow, C. Kirschbaum, K. Greis, C. Manz and K. Pagel, Chem. Rev., 2022, 122, 7840–7908.
21 P. E´cija, I. Uriarte, L. Spada, B. G. Davis, W. Caminati, F. J. Basterretxea, A. Lesarri and E. J. Cocinero, Chem. Commun., 2016, 52, 6241–6244.
22 C. Calabrese, I. Uriarte, A. Insausti, M. Vallejo-Lo´pez, F. J. Basterretxea, S. A. Cochrane, B. G. Davis, F. Corzana and E. J. Cocinero, ACS Cent. Sci., 2020, 6, 293–303.
23 B. Schindler, L. Legentil, A.-R. Allouche, V. Ferrie`res and I. Compagnon, Phys. Chem. Chem. Phys., 2019, 21, 12460–12467.
24 J. S. Ho, A. Gharbi, B. Schindler, O. Yeni, R. Bre´dy, L. Legentil, V. Ferrie`res, L. L. Kiessling and I. Compagnon, J. Am. Chem. Soc., 2021, jacs.0c11919.
25 B. Favreau, O. Yeni, S. Ollivier, J. Boustie, F. L. De´ve´hat, J.-P. Gue´gan, M. Fanuel, H. Rogniaux, R. Bre´dy, I. Compagnon, D. Ropartz, L. Legentil and V. Ferrieres, Synthesis of an Exhaustive Library of Naturally Occurring Galf-Manp and Galp-Manp Disaccharides. Towards Fingerprinting According to the Ring Size by Advanced Mass Spectrometry-Based IM-MS and IRMPD., J. Org. Chem., 2021, 86(9), 6390–6405.
26 B. Kirchner, J. Blasius, L. Esser and W. Reckien, Adv. Theory Simul., 2021, 4, 2000223.
27 J. J. P. Stewart, MOPAC2012 2012.
28 C. J. Gray, B. Schindler, L. G. Migas, M. Picˇmanova´, A. R. Allouche, A. P. Green, S. Mandal, M. S. Motawia, R. Sa´nchez-Pe´rez, N. Bjarnholt, B. L. Moller, A. M. Rijs, P. E. Barran, I. Compagnon, C. E. Eyers and S. L. Flitsch, Anal. Chem., 2017, 89, 4540–4549.
29 A. D. Hill and P. J. Reilly, J. Chem. Inf. Model., 2007, 47, 1031–1035.
30 D. Cremer and J. A. Pople, J. Am. Chem. Soc., 1975, 97, 1354–1358.
31 C. Altona and M. Sundaralingam, J. Am. Chem. Soc., 1972, 94, 8205–8212.
32 A. D. Becke, J. Chem. Phys., 1993, 98, 1372–1377.
33 A. D. Becke, Phys. Rev. A: At., Mol., Opt. Phys., 1988, 38, 3098–3100.
34 C. Lee, W. Yang and R. G. Parr, Phys. Rev. B: Condens. Matter Mater. Phys., 1988, 37, 785–789.
35 T. Yanai, D. P. Tew and N. C. Handy, Chem. Phys. Lett., 2004, 393, 51–57.
36 A.-R. Allouche, J. Comput. Chem., 2011, 32, 174–182.

37 M.-P. Gaigeot, M. Martinez and R. Vuilleumier, Mol Phys, 2007, 105, 2857–2878.
38 K. Gaweda and W. Plazinski, Org. Biomol. Chem., 2019, 17, 2479–2485.
39 GLYCOPEDIA, https://glycopedia.eu/e-chapters/symbolic-representation-of-monosaccharides-in-the-age-of-glycobiology/120-Monosaccharides, (accessed September 21, 2022).